Constrained Formation Control Framework for Spacecraft Proximity Formation Flight

Available online at www.sciencedirect.com

ScienceDirect

IFAC Papers Online CONFERENCE PAPER ARCHIVE

IFAC PapersOnLine 59-31 (2025) 37–42

Constrained Formation Control Framework for Spacecraft Proximity Formation Flight

D. Ruggiero * **P. Bertuccio** * **E. Capello** *

* *Politecnico di Torino, Torino, Italy (e-mail:dario.ruggiero@polito.it, pierantonio.bertuccio@polito.it, elisa.capello@polito.it).*

Abstract: This paper presents an analytical framework for designing Artificial Potential Field (APF) gains for spacecraft formation control within the Circular Relative Orbit framework. While APF methods are effective for formation shaping, they often overlook system dynamics and constraints, risking instability. The proposed method ensures Lyapunov stability through a systematic gain design and the definition of an operational bound. Stability is verified using Structured Singular Value μ-analysis. Numerical simulations confirm the robustness and scalability of the approach, supporting safe and reliable proximity operations for future multi-satellite missions in Earth orbit.

Keywords:
Formation control, Autonomous systems, Multi-agent systems, Guidance and control, Space systems

1. INTRODUCTION

Proximity formation flight of spacecraft represents a critical capability for a range of future space missions, including distributed satellite systems, in-orbit servicing, and space-based interferometry. The ability of multiple spacecraft to maintain prescribed relative configurations while operating in close proximity requires precise formation control strategies that are robust, scalable, and safe.

In (Ito, 2024, 2025), formation flight in Earth orbit is proposed as a cost-effective and practical platform for advancing the development and testing of new spacecraft technologies. Earth orbit formation flight offers a unique and accessible environment for testing and validating advanced spacecraft technologies and control algorithms. Acting as a virtual laboratory, it enables researchers to experiment with innovative formation control strategies, sensing techniques, and autonomous operations in realistic conditions, accelerating the development of next-generation space systems. In (Ruggiero et al., 2024) the design of a proximity formation flight framework for Earth orbit is proposed. It is based on the definition of a Circular Relative Orbit (CRO) framework consisting of an optimal circular relative trajectory around a target. CRO-based missions are of particular interest because they enable fuel-efficient relative motion, simplify the design of autonomous GNC algorithms, and provide a scalable framework for safe formation deployment and multi-spacecraft operations. In (Ruggiero et al., 2025), this framework is deeply analyzed designing a guidance law for approaching, tracking and guaranteeing CRO tracking under actuators constraints, achieving robust, scalable and number-varying formation flight. The formation control consists of a Artificial Potential Field (APF) approach based on shaping functions (Izzo and Pettazzi, 2005; Saaj et al., 2006). However, this method needs to be carefully designed in order to not lead to instability. The APF strategies generally neglect system dynamics and actuator constraints, which can lead to unstable or unsafe behavior if not properly addressed. Moreover, tuning APF gains is inherently challenging, as improper selection can lead to local minima and may require scenario-specific adjustments to ensure reliable performance across different mission conditions.

In this paper, the design of APF gains for formation control is addressed within the CRO framework. The CRO framework provides a systematic representation of the relative dynamics and operational constraints, enabling a robust and consistent formulation of the guidance parameters. The proposed analysis is supported by both analytical derivations and numerical simulations. In particular, an operational bound is defined to ensure satisfaction of Lyapunov stability conditions for CRO tracking, and its validity is further verified through Structured Singular Value (SSV) μ-analysis. By formulating the formation control problem with explicit consideration of relative dynamics and constraints, the CRO framework offers a systematic and verifiable method for safe and reliable proximity operations. Paper contribution is: (i) the analytical formulation for the design of APF gains for formation control within the CRO framework, and ensuring stability and constraint satisfaction, and (ii) the definition of an operational bound that guarantees Lyapunov stability for CRO tracking under actuator limitations. This work aims to provide a rigorous foundation for the design of APF-based formation controllers that are both analytically grounded and practically implementable within the CRO framework. The proposed methodology enhances the reliability and scalability of proximity operations, paving the way for more autonomous and adaptable multi-spacecraft missions in Earth orbit.

2. FORMATION FLIGHT IN CIRCULAR RELATIVE ORBIT

This paper focuses on formation flight in the CRO framework. CROs consist of a class of relative trajectories, and offer a structured framework for the design of multi-satellite formations operating in Earth orbits. In a CRO, each deputy spacecraft maintains a bounded trajectory around a centered chief spacecraft, resulting in periodic relative motion with fixed geometry. This structure provides geometric predictability, supports continuous visual or sensing contact, and simplifies

10.1016/j.ifacol.2026.01.058

onboard implementation of relative guidance and control strategies. The dynamical model adopted in this work assumes a circular chief orbit and leverages the Hill–Clohessy–Wiltshire (HCW) equations to describe the relative dynamics in the Local-Vertical Local-Horizontal (LVLH) frame. Within this linearized setting, CROs correspond to closed-form solutions that are fully defined by initial conditions and orbital parameters, offering an ideal testbed for control design.

Stability analysis of CRO tracking is central to the guidance strategy. The problem is formulated as a velocity tracking task, where the control objective is to regulate the deputy's velocity relative to the CRO reference. Stability margins are characterized in terms of the maximum allowable tracking error, bounded by actuation limits. This approach enables a quantitative connection between propulsion capability and guidance feasibility, establishing the operational envelope for control design. Equations (1–3) follow the derivation presented in (Ruggiero et al., 2025), which provides the basis for the following discussion.

Assumption 1. The spacecraft is close to the desired CRO trajectory. The actuators thrust is limited by $\|a\|_\infty \leq U$, and disturbances are bounded by $\|w\|_\infty \leq W$, with $U > W$.

Proposition 1. The problem of tracking a CRO trajectory is inherently linked to actuator limitations. These constraints define the operative bounds within the closed-loop system can guarantee convergence to the CRO trajectory and closed-loop system stability. Defining the CRO tracking error $\delta = \|v - v_{CRO}\|_\infty$, the closed-loop system stability is guaranteed if

$$\delta(t=0) < \frac{6(U-W)}{\omega(3+\sqrt{3})} = \bar{\Delta}. \tag{1}$$

The CRO radius plays a critical role in defining the trade-offs between maneuverability, control effort, and stability. Larger radii entail higher relative velocities, increasing fuel consumption and reducing the robustness to actuation constraints and modeling inaccuracies. In practice, there exists an infinite set of CRO trajectories corresponding to a different radius

$$\mathcal{CRO} = \left\{ R > 0 \quad | \quad p(t) = R \begin{bmatrix} -\cos(\omega t) \\ \frac{\sqrt{3}}{2}\sin(\omega t) \\ \frac{1}{2}\sin(\omega t) \end{bmatrix} \right\}. \tag{2}$$

In (Ruggiero et al., 2025) an Adaptive Lyapunov Guidance Vector Field (A-LGVF) approach is proposed to guarantee the tracking of a limited set of CRO trajectories. For a comprehensive understanding, the guidance algorithm for CRO tracking is reported in Appendix A. In *Proposition 1*, the tracking stability is inherently tied to the maximum velocity error between the spacecraft and the current CRO trajectory. The A-LGVF approach guarantees that this condition is always satisfied against actuators constraints, orbital and environment perturbations (in accordance with *Assumption 1*), regulating the CRO radius to minimize δ, and guaranteeing $\delta(t) < \eta\bar{\Delta}$.

Within the CRO framework, formation flight can be effectively formulated as a control problem constrained by velocity budget limitations. The A-LGVF generates a velocity field v_d^{CRO} leading the system to track the desired CRO. This framework can be easily integrated with APF-based methods to address complex scenario (i.e., formation control, collision avoidance). However, the APF function acts as a perturbation

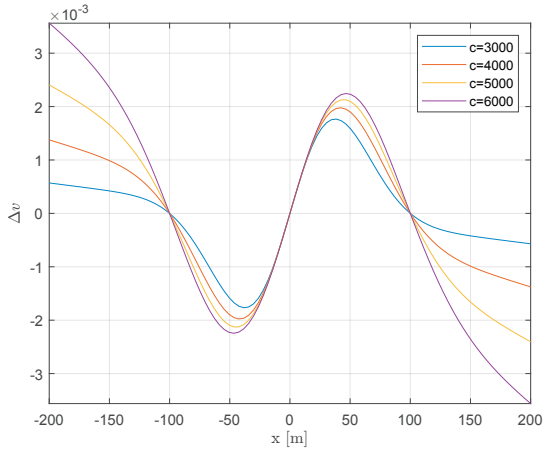

Fig. 1. Formation attraction function (1D), illustrating the potential that drives each spacecraft toward the desired spacing along the line-of-sight.

$v_d = v_d^{CRO} + \Delta v_{ff}$ for the CRO tracking stability. For this reason, it is essential for Δv_{ff} to be bounded by

$$\Delta v_{ff} \leq \alpha\bar{\Delta}, \tag{3}$$

with $\alpha + \eta \leq 1$. APF-function's gains are generally trivial to design for balancing performance while avoiding local-minima. In this paper, this problem is addressed by exploiting the definition and the characteristics of the CRO trajectory.

3. FORMATION CONTROL

In this section, the design of the APF-based formation control algorithm is addressed. The guidance function is based on the equilibrium shaping method, described in (Izzo and Pettazzi, 2005; Saaj et al., 2006). This leads to the definition of an attractive-repulsive function with the purpose to reach the desired spacecraft separation distance. In practice, it is expressed by a velocity field acting on the line-of-sight of the two (or more) systems

$$\Delta v_{ar} = -\sum_{j}^{N-1} p_j b \left(e^{-\frac{d^2}{c}} - e^{-\frac{p_j^T p_j}{c}} \right) \tag{4}$$

where $p_j \in \mathbb{R}^3$ is the relative position vector pointing to j-th spacecraft, and $b,c > 0$ are constant gains, and d is the desired separation distance. Tracking the velocity field makes the spacecraft reach the desired separation distance. Gain design is based on the characterization of the function for the one dimensional (1D) case, acting in line-of-sight. The linearization around the origin of Equation (4) leads to

$$\Delta v_{ar} \simeq b\left(1 - e^{-\frac{d^2}{c}}\right) x \tag{5}$$

Considering the limitation of the linearized function in the interval $x \in [-d^*, d^*]$, where $x = d^*$ corresponds to the maximum of Equation (4) in the interval $[0,d]$, it is possible to design b such to have

$$|\Delta v_{ar}| \leq \bar{\Delta v} \qquad \rightarrow \qquad b \leq \frac{\bar{\Delta v}}{\left(1 - e^{-\frac{d^2}{c}}\right) d^*}. \tag{6}$$

The design of c is based on qualitative representation of Equation (4) for the 1D case, Figure 1, where b is designed according to Equation (6). Considering the simplified 1D system, tracking the velocity field given in Equation (4) with a feedback controller $u = -k(\dot{x} - \Delta v_{ar})$, leads to the harmonic system

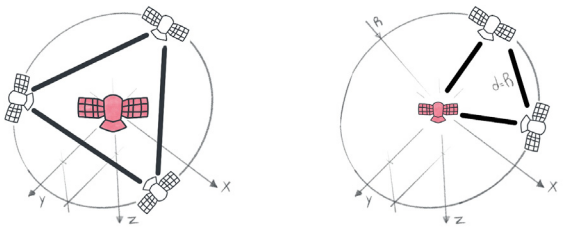

Fig. 2. Example of centralized and decentralized triangular formations.

$$\ddot{x} = -k\dot{x} - \omega_n^2 x, \tag{7}$$

where ω_n^2 is evaluated linearizing the system in proximity of $x \simeq d$, and it is given by

$$\omega_n^2 = 2k\frac{bd^2}{c}e^{-d^2/c}. \tag{8}$$

However, limiting the formation control to this contribution leads to long settling time. Settling performance can be improved augmenting Equation (4) with a term based on formation center. This term is designed using an attractive-parabolic APF function given as

$$G_{fc} = \frac{1}{2}k_{att}(R_m - R_{m,d})^2 \tag{9}$$

where $k_{att} > 0$ is an attractive gain, R_m is the radius of the formation center with respect to the LVLH reference frame, with $p_m = p + \sum_j p_j$ and $R_m = \|p_m\|_2$, and $R_{m,d}$ is the desired formation center radius. With $R_{m,d} = 0$ the formation is centered in the LVLH reference frame, while for $R_{m,d} > 0$ it is possible to achieve decentralized triangular formations (see Figure 2). In centralized triangular formations, the formation is centered in the LVLH reference frame, corresponding to a target (real or virtual). In the decentralized formation, the LVLH reference frame is centered in one spacecraft, while the others move on the CRO trajectory with radius $R = d$.

Considering the simplified 1D system, tracking the augmented velocity field ($\Delta v - \nabla G_{fc}$, with $R_{m,d} = 0$) leads to the harmonic system given in Equation (7), with

$$\omega_n^2 = k\left(2\frac{bd^2}{c}e^{-d^2/c} + k_{att}\right). \tag{10}$$

This allows to reduce the settling time up to 96%, improving significantly the performance of the algorithm. Moreover, the inclusion of the term associated with the formation center simplifies the planar formation control problem by introducing a component orthogonal to the line-of-sight direction, which enhances formation spatial distribution. For these reasons, the final formulation of the formation control velocity field is given by

$$\Delta v_{ff} = -\sum_{j}^{N-1} p_j b\left(e^{-\frac{d^2}{c}} - e^{-\frac{p_j^T p_j}{c}}\right) + \\ -k_{att}\left(1 - \frac{R_{m,d}}{R_m}\right)\frac{(p + \sum_j p + p_j)}{N}. \tag{11}$$

With respect to the CRO tracking problem, the formation control contribution acts as a disturbance. The condition to guarantee the stability of the closed-loop system (*Proposition 1*) is tight due to the actuators limitations. Moreover, moving outside of the CRO trajectory increases significantly fuel consumption. In order to limit the effect of the formation

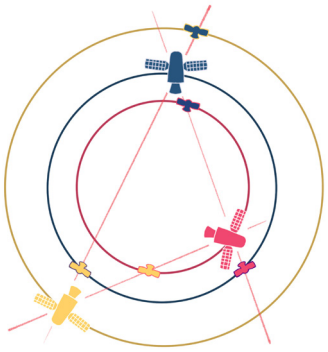

Fig. 3. Projection of the neighboring spacecraft positions onto the CRO trajectory.

control contribution in destabilizing the formation, Equation (11) is evaluated considering j-th spacecraft in-plane projection along the line-of-sight on the current CRO trajectory. This is showed in Figure 3, where the colored dots denote the projection. This approach results in two major benefits:

(1) The projection in the CRO plane avoid spacecraft to drift outside the plane, as a benefit for stability.
(2) The projection on the CRO trajectory reduce the generation of reactive maneuvers in the radial direction, that may destabilize the spacecraft.

Although the proposed approach enhances formation stability, it may increase exposure to potential collisions. However, this risk is mitigated by the collaborative nature of the formation framework, where all spacecraft follow a shared protocol to reach the target separation and converge toward the formation center in a coordinated manner. As a result, collision are effectively avoided. In this framework, the desired separation distance d is not constant, but it directly related to the CRO radius $R(t)$, which is given by the A-LGVF algorithm. Separation distance is determined by

$$d = \begin{cases} R\sqrt{3} & \text{for a cen. triangular formation} \\ R & \text{for a dec. triangular formation} \end{cases}. \tag{12}$$

This framework allows to identify formation control bounds within the operational envelope. The maximum available budget for formation control is given by $\alpha\bar{\Delta}$, from Equation (3). Since Δv_{ff} is expressed by N contributions, where N is the number of spacecraft in formation, the maximum value of each contribution is designed as

$$\bar{\Delta v} = \frac{\alpha\bar{\Delta}}{N}. \tag{13}$$

Attractive-repulsive term is designed according to Equation (6). Figure 4 illustrates the attractive-repulsive term within the operational envelope, and designed based on the desired spacecraft separation distance (i.e., $d = 100$ m). The plot shows how the tracking velocity varies with time-varying values of $d = d(R)$, while keeping parameters b and c fixed. This contribution is continuous with respect to d, and bounded by $\bar{\Delta v}$. The formation center attraction term is maximized by $k_{att}p_m \leq k_{att}R(t) \leq \bar{\Delta v}$, which is verified for

$$k_{att} \leq \frac{\alpha\bar{\Delta}}{NR(t)} \leq \frac{\alpha\bar{\Delta}}{N\underline{R}}. \tag{14}$$

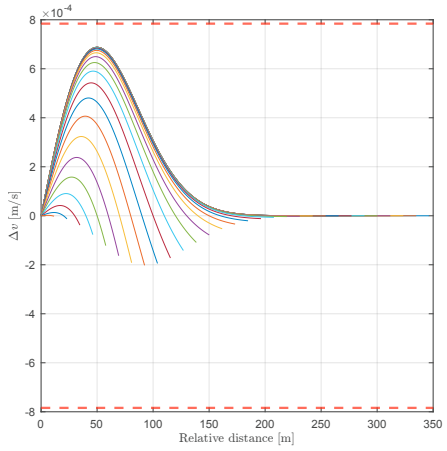

Fig. 4. Attractive–repulsive potential term contribution evaluated for the case of a time-varying desired separation distance $d=d(R)$, highlighting its effect on the evolution of the inter-spacecraft spacing.

This framework enables the design of the APF method in a way that guarantees compliance with stability conditions throughout the operational envelope.

4. NUMERICAL ANALYSIS

Stability conditions are extended to realistic operational scenarios by incorporating uncertainties in radial motion through robust stability analysis. In this context, μ-analysis is employed as a performance index to assess the effectiveness of guidance parameter selection. It consist of a typical linear tool for stability verification. First, the system is exploited by the linear fractional transformation, as in (Doyle, 1982). As shown in Figure 5, the standard $M-\Delta$ configuration is considered, where the uncertainties matrix $\Delta(s)$ is connected to the given system $M(s)$, defining the feedback connection $F(M,\Delta)$. Following the SSV principle, the feedback connection $F(M,\Delta)$ robust stability is guaranteed if

$$\sup_{\tilde{\omega}\in\mathbb{R}}\{\mu_{\Delta}(M(j\tilde{\omega}))\}\leq 1 \tag{15}$$

at each given frequency $\tilde{\omega}$, where $\mu_{\Delta}(M)$ is the SSV, and it is defined as

$$\mu_{\Delta}(M)=\frac{1}{\sup_{\Delta\in\Delta^{*}}\{\Delta \mid \det(I-M\Delta)\neq 0\}}, \tag{16}$$

where Δ^{*} is the set of values that takes account of the possible bounded variation of Δ. In practice, it is not always possible to analytically compute SSV margin expressed in Equation (15). For this reason, typical solution is to rely on numerical approaches, as shown in (Gu et al., 2005; Young et al., 1991).

The CRO trajectory tracking is formulated as a velocity tracking problem

$$e=\left[v-v_{d}^{CRO}(p)\right]. \tag{17}$$

Error dynamics is determined as

$$\dot{e}=\left[\dot{v}-\dot{v}_{d}^{CRO}(p)\right], \tag{18}$$

but, in proximity of the CRO trajectory, it is given as the linear relationship

$$\dot{e}=\begin{bmatrix}0 & 0 & 0\\ \frac{\sqrt{3}}{2}\omega & 0 & 0\\ -\frac{3}{2}\omega & 0 & 0\end{bmatrix}e+u, \tag{19}$$

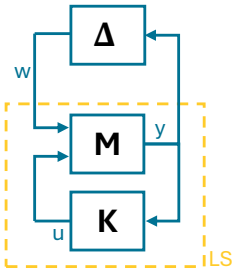

Fig. 5. Block diagram representation of the feedback interconnection between the nominal system matrix M and the structured uncertainty block Δ, as used in the μ-analysis framework to assess robustness against model uncertainties.

with $u=-K(e+\Delta v_{ff})$. However, the linear approximation does not account for residual radial velocity and saturation effect. The effect of saturation is given by

$$\Delta_{sat}=\begin{cases}(|K(e+\Delta v_{ff})|-U)\text{sign}(e) & \text{if } u\geq U\\ 0 & \text{if } u<U\end{cases} \tag{20}$$

The radial velocity affect directly the tracking error $e\simeq e+\Delta_{\dot{r}}$. For the A-LGVF the radial velocity is bounded by the definition of the adaptive function gains, and in particular by Equation (A.6) as

$$\Delta_{\dot{r}}\leq\frac{\beta}{1-\epsilon/\eta}+\alpha\bar{\Delta}. \tag{21}$$

Since the nonlinearities in the closed-loops system cannot be directly accounted in the robustness stability analysis, they are included using the simplified approach proposed in (Pagone et al., 2020; Mancini and Ruggiero, 2025). In particular, the nonlinear uncertainty is included by evaluating the input-output gain of Δ_{NL}, defined as the induced norm of the nonlinear terms in the closed-loop system. The input-output relationship with the linearized plant is evaluated through

$$||\Delta_{NL}||_{\infty}=\sup_{y\neq 0}\frac{||w||_{\infty}}{||y||_{\infty}}. \tag{22}$$

This allows to incorporates the robust stability analysis with the nonlinearities related to unmodeled dynamics. Rigorous derivation of a global norm bound for Δ_{NL} is challenging, and require extensive data across an infinite-dimensional space. Indeed, the proposed approach is based on the approximation of the nonlinear terms based on the model physical and operational bounds, and the specific characteristics of the guidance and control algorithms. This provides a practical, albeit local, approximation of the nonlinear uncertainties within the expected operational envelope.

Following the approximation given in Equation (22), the uncertainties Δ_{sat} and $\Delta_{\dot{r}}$ affect the system as constant feedback approximations:

$$\dot{e}=\begin{bmatrix}0 & 0 & 0\\ \frac{\sqrt{3}}{2}\omega & 0 & 0\\ -\frac{3}{2}\omega & 0 & 0\end{bmatrix}e-Ke+(\|\Delta_{sat}\|_{\infty}+\|\Delta_{\dot{r}}\|_{\infty})e \tag{23}$$

where the values are expressed as

$$\begin{cases}\|\Delta_{sat}\|_{\infty}= & k-\dfrac{U}{\bar{\Delta}\eta+\alpha\bar{\Delta}}\\ \|\Delta_{\dot{r}}\|_{\infty}= & \dfrac{k\beta/(1-\epsilon/\eta)+\alpha\bar{\Delta}}{\bar{\Delta}}\end{cases} \tag{24}$$

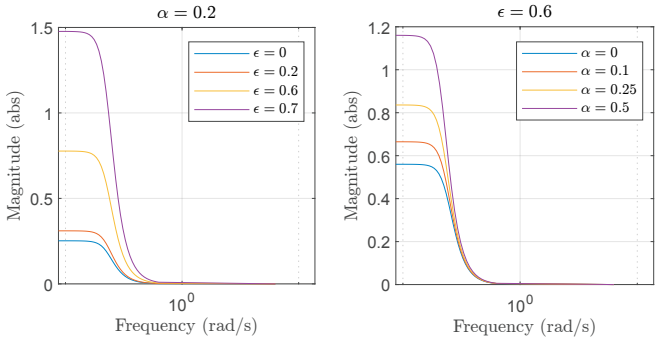

Fig. 6. μ-analysis performed to identify the critical parameters affecting closed-loop stability and performance. The plot highlights the sensitivity of the GNC framework to α and ϵ design, and provides a qualitative measure of robustness margins.

Table 1. Guidance and Control parameters

Parameter	Value	Parameter	Value
η	0.8	c	5000
ϵ	0.6	b	8.90×10^{-5}
γ	2.08×10^{-4}	k_{att}	1.66×10^{-4}
G	0.97	U	10×10^{-6}
k	1	W	$1\times10^{-6.5}$

This approach provides a conservative representation that encapsulates the expected closed-loop system behavior. Upper bound of μ is reported in Figure 6, with $k = 1$ and $\eta = 0.8$. The A-LGVF stability is independent to the CRO radius, but related to the selection of ϵ. Results highlight the existence the critical value of ϵ to be $0.6 < \epsilon_{max} < 0.7$. However, even if the proposed analysis allows to extend the robust stability considerations to the nonlinear system, identifying the critical design that may bring the system to instability, it is not a rigorous analysis. μ-analysis provides a qualitative indication on the closed-loop system design limits in tracking CRO trajectories while dealing with formation control.

In compliance with the results achieved with the μ-analysis, a dedicated simulation campaign is conducted to evaluate the responsiveness and stability of the proposed guidance strategies in formation flight. The simulation campaign focus on spacecraft operations in proximity of the desired configuration (with an error of m and mms^{-1} for position and velocity, respectively). Figure 7 illustrates the settling behavior of a triangular formation. The plots show the time evolution of the inter-spacecraft separation distance (top) and the CRO radius (bottom), providing insight into the system's ability to achieve and maintain the desired triangular configuration. Two scenarios are compared: a target separation distance of 100 m (red) and 50 m (blue). The simulations account for the complete guidance and control architecture, including deviations in CRO tracking, and with random LEO orbit selection $r_o \in [7000, 8371]$ km and disturbances. These plots provide insight into the transient dynamics of the system. In particular, they reveal the impact of guidance design on formation settling time, validating the effectiveness of the proposed framework under realistic operational conditions. Guidance and control parameters are summarized in Table 1. Simulation campaign leads to longer settling times (~6 h) with respect to theoretical analysis (~2.5 h, from Equation (10)). This is due to the combination of CRO tracking and formation control coupling, leading to longer transient. The analysis demonstrates that

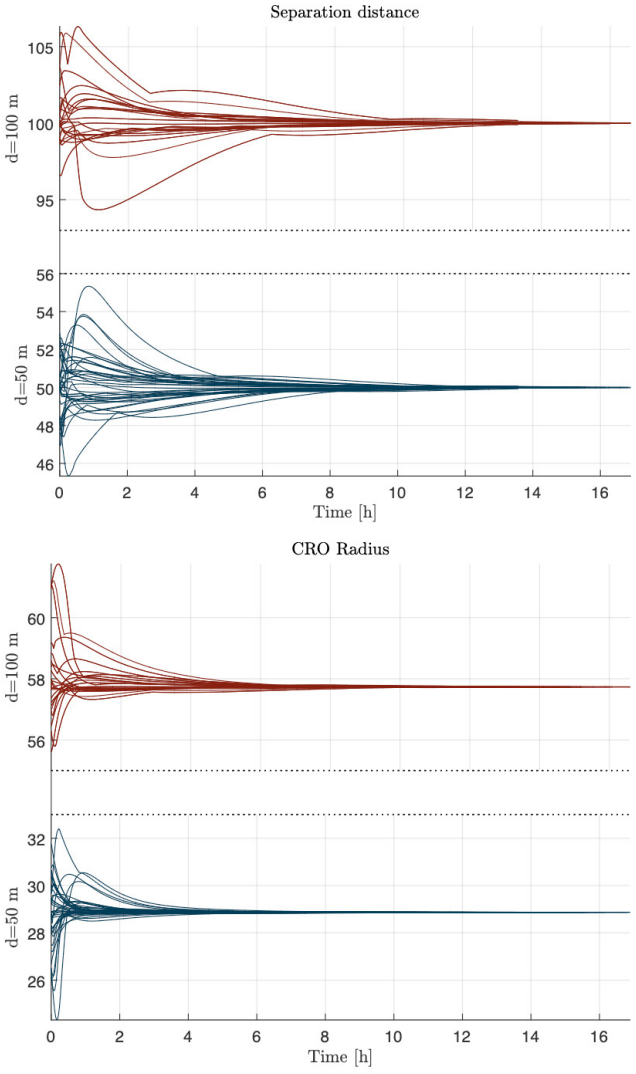

Fig. 7. Simulation campaign conducted to evaluate the settling time of a centralized triangular formation. The results illustrate the ability of the proposed guidance and control framework to autonomously achieve the desired configuration within bounded convergence times.

increasing the CRO radius leads to longer settling times. This is due to the higher orbital velocities associated with larger radius, which result in more demanding maneuvering conditions. Consequently, the guidance system must work harder to regulate deviations and achieve convergence, highlighting the sensitivity of formation response to the selected CRO scale. By accounting for both control limitations and inter-satellite interactions, the approach ensures robust and safe formation maintenance within the intended mission constraints.

5. CONCLUSIONS

This paper presented a constrained formation control framework for spacecraft proximity operations based on APF within the CRO framework. The primary contribution is the analytical formulation of APF gain design that ensures Lyapunov stability. The CRO model provided a systematic foundation for incorporating dynamic behavior and constraint handling into the guidance law. An operational bound was derived to guarantee stable tracking, and its effectiveness was

verified through SSV μ-analysis and numerical simulations. The results demonstrated the robustness, scalability, and safety of the proposed method across various formation scenarios. The developed framework supports the deployment of more autonomous, reliable, and adaptable multi-spacecraft systems in Earth orbit and lays the groundwork for experimental validation and extension to more complex mission architectures. Future work will focus on real-time implementation, distributed control architectures, and hardware-in-the-loop testing to further mature the proposed approach.

ACKNOWLEDGEMENTS

This study was carried out within the Space It Up project funded by the Italian Space Agency, ASI, and the Ministry of University and Research, MUR, under contract n. 2024-5-E.0 - CUP n. I53D24000060005.

REFERENCES

Doyle, J. (1982). Analysis of feedback systems with structured uncertainties. In *IEE Proceedings D (Control Theory and Applications)*, volume 129, 242–250. IET Digital Library.

Gu, D.W., Petkov, P., and Konstantinov, M.M. (2005). *Robust control design with MATLAB®*. Springer Science & Business Media.

Ito, T. (2024). Formation-flying interferometry in geocentric orbits. *Astronomy & Astrophysics*, 682, A38.

Ito, T. (2025). Precise formation flying in low earth orbit under environmental and systematic uncertainties. *Acta Astronautica*.

Izzo, D. and Pettazzi, L. (2005). Equilibrium shaping: distributed motion planning for satellite swarm. In *Proc. 8th Intern. Symp. on Artificial Intelligence, Robotics and Automation in space*, volume 25.

Lahana, Y., Mancini, M., Peaucelle, D., Capello, E., and Evain, H. (2023). Comparison of adaptive control laws on a satellite attitude control benchmark. In *2023 9th International Conference on Control, Decision and Information Technologies (CoDIT)*, 1–6. IEEE.

Lawrence, D., Frew, E., and Pisano, W. (2007). Lyapunov vector fields for autonomous uav flight control. In *AIAA Guidance, Navigation and Control Conference and Exhibit*, 6317.

Mancini, M. and Ruggiero, D. (2025). Artificial potential field and sliding mode control for spacecraft attitude maneuver with actuation and pointing constraints. *Control Engineering Practice*, 162, 106373.

Pagone, M., Novara, C., Martella, P., and Nocerino, C. (2020). Gnc robustness stability verification for an autonomous lander. *Aerospace Science and Technology*, 100, 105831.

Ruggiero, D., Ito, T., Capello, E., and Tsuda, Y. (2024). Feasibility study on lgvf for spacecraft formation flight mission. In *2024 SICE Festival with Annual Conference (SICE FES)*, 595–600. IEEE.

Ruggiero, D., Ito, T., Capello, E., and Tsuda, Y. (2025). Adaptive guidance for low-thrust formation flight mission in circular relative orbit. *Acta Astronautica*.

Saaj, C.M., Lappas, V., and Gazi, V. (2006). Spacecraft swarm navigation and control using artificial potential field and sliding mode control. In *2006 IEEE International Conference on Industrial Technology*, 2646–2651. IEEE.

Yao, P., Wang, H., and Su, Z. (2015). Real-time path planning of unmanned aerial vehicle for target tracking and obstacle avoidance in complex dynamic environment. *Aerospace Science and Technology*, 47, 269–279.

Young, P.M., Newlin, M.P., and Doyle, J.C. (1991). Mu analysis with real parametric uncertainty. In *[1991] Proceedings of the 30th IEEE Conference on Decision and Control*, 1251–1256. IEEE.

Appendix A. CRO TRACKING GUIDANCE

The CRO is defined as a circular trajectory in an inclined plane. The CRO reference frame is defined from the rotation of an angle $\phi=\pi/6$ around the x-axis of the LVLH reference frame. The rotation matrix from the CRO to the LVLH reference frame is defined as

$$Q_{CRO}^{LVLH}=\begin{bmatrix}1 & 0 & 0\\ 0 & \cos(\phi) & -\sin(\phi)\\ 0 & \sin(\phi) & \cos(\phi)\end{bmatrix} \tag{A.1}$$

The CRO attraction function is designed in the CRO reference frame, and starting from the LGVF algorithm introduced in (Yao et al., 2015; Lawrence et al., 2007). Final formulation of the velocity field is expressed as

$$\begin{cases} r=\sqrt{x^{*2}+y^{*2}} \\ \delta^*=\dfrac{nR}{r\sqrt{(r^2+R^2)^2+\lambda(z^{*2}-H^2)^2}} \\ u^*=\delta^*\left[-x^*(r^2-R^2)+2y^*rR\right] \\ v^*=\delta^*\left[-y^*(r^2-R^2)-2x^*rR\right] \\ w^*=\delta^*[-\lambda r(z^*-H)] \end{cases} \tag{A.2}$$

where $p^*=[x^*,\ y^*,\ z^*]^T$ is the spacecraft position in the CRO reference frame, n and R are the CRO parameters, and $\lambda>0$ is a constant gain. In the LVLH reference frame, the tracking velocity is given as

$$v_d^{CRO}=Q_{CRO}^{LVLH}[u^*\ \ v^*\ \ w^*]^T \tag{A.3}$$

The main characteristic of the proposed guidance is that the desired velocity is normalized, and $||v_d^{CRO}||_2=nR$. An adaptive law based on (Lahana et al., 2023) is included to cope with actuators limitations. The adaptive law regulates the desired CRO radius R variation, from the initial value R_i to the final value R_d, according to the actual state of system. This relationship is expressed by

$$\begin{aligned}\dot{R}=\text{Proj}_{[\underline{R},\bar{R}]}[-G\|v-v_d^{CRO}\|_\infty\text{sign}(\partial v)+ \\ -\gamma(R-R_d)],\end{aligned} \tag{A.4}$$

where $\partial v=\omega R-\|v\|_2$, $\underline{R}\leq\min(R_i,R_d)$ and $\bar{R}\geq\max(R_i,R_d)$, and $G,\gamma>0$ are constant gains, designed as

$$G\geq\gamma\frac{\bar{R}-\underline{R}}{\eta\bar{\Delta}} \qquad \text{and} \qquad \gamma\leq\frac{\beta}{\bar{R}-\underline{R}} \tag{A.5}$$

with $\beta=\sqrt{3}U/(3\omega)$. In practice, the maximum $\dot{R}$ value is related to $R=\underline{R}$ and $\delta=0$. Therefore, the proposed design is really conservative, and it leads to long maneuvering times. Time-performance trade off is achieved considering an intermediate design condition, $\delta=\epsilon\bar{\delta}$. It is expressed by

$$\dot{R}\leq\gamma^*\left[-\frac{\bar{R}-\underline{R}}{\eta\bar{\delta}}\epsilon\bar{\delta}+(\bar{R}-\underline{R})\right] \tag{A.6}$$

which leads to

$$\gamma\leq\gamma^*\leq\frac{\beta}{(\bar{R}-\underline{R})(1-\epsilon/\eta)} \tag{A.7}$$

with $0\leq\epsilon<\eta$. Closer is ϵ/η to 1, higher is the possibility to have the controller operating in proximity of the saturation bounds.